Physica C 220 (1994) 195–202
North-Holland

PHYSICA C

Quasiparticle injection effects in $YBa_2Cu_3O_x$-based planar structures at high operating temperatures

Yu.M. Boguslavskij [1], K. Joosse, A.G. Sivakov [2], F.J.G. Roesthuis, G.J. Gerritsma and H. Rogalla

Department of Applied Physics, University of Twente, PO Box 217, 7500 AE Enschede, The Netherlands

Received 26 August 1993
Revised manuscript received 2 October 1993

The modulation of the supercurrent I_s of a YBCO bridge by the quasiparticle-injection current I_G from the YBCO/Au or YBCO/PBCO/Au junctions at temperatures of 60–85 K is determined by two effects: (1) summation of the currents I_S and I_G in the YBCO bridge, and (2) nonequilibrium suppression of I_S by the quasiparticle injection. At a thickness of the PBCO barrier of 40 nm the modulation of I_S can be described by the current-summation effect only. For YBCO/Au structures the current gain $\Delta I_S/\Delta I_G$ increases linearly with decreasing temperature, reaching the value of 2 at 60 K. Numerical simulations of the current–voltage characteristics show an increase of the effective temperature T^* of the YBCO bridge under injection only at small thicknesses of the PBCO barrier. Visualization of the voltage drop over the junction area by laser scanning microscopy shows a qualitative agreement with the electrical measurements with respect to the current summation and nonequilibrium effects.

1. Introduction

The nonequilibrium behavior of high-T_c superconductors (HTS's) under external quasiparticle or phonon injection, optical or microwave irradiation has both a scientific and a practical interest. The low carrier density $N(0) \sim 6 \times 10^{21}$ cm^{-3} is an advantage of HTS's for the sensitive response to an external influence. However, the creation of a nonequilibrium state at high operating temperatures is rather complicated for several reasons. An increase of the operating temperature increases the density of thermal quasiparticles N_T. This decreases the nonequilibrium effects for the same levels of injection or irradiation. Second, the critical current density J_s in HTS's is determined by flux creep with a low activation energy, which becomes of major importance especially at high temperatures. Zeldov et al. [1] showed that under optical irradiation at temperatures close to T_c the response of epitaxial $YBa_2Cu_3O_x$ (YBCO) films corresponds to a nonequilibrium optical enhancement of the flux creep. The behavior of HTS structures under quasiparticle injection at high temperatures and the reasons for a J_c suppression – creation of excess quasiparticles or phonons, activation of the flux motion, heating, or other effects – has not been analyzed yet.

Due to structural simplicity, large current and voltage gain and relatively high operating speed, the injection-controlled structures are promising for practical applications like switching or transistor-like elements. A current gain of 95 was found in low-T_c weak-link structures [2,3]. A first study of quasiparticle injection in HTS YBCO/Al structures shows a current gain of 5–7 at 4.2 K [4].

We have investigated the modulation of the supercurrent I_s of YBCO bridges by an injection current from YBCO/Au or YBCO/PBCO/Au junctions at temperatures of 60–85 K, as we reported briefly in ref. [5]. A current gain $K_G = \Delta I_C/\Delta I_G$ of 1.5 at 65 K was obtained for YBCO/Au structures. In this paper we analyze the reasons for the supercurrent modulation in YBCO/Au and YBCO/PBCO/Au planar structures. A nonuniform current

[1] On leave from Institute of Metal Physics, Kiev, Ukraine.
[2] On leave from Institute for Low Temperatures, Kharkov, Ukraine.

SSDI 0921-4534(93)E0821-H

density in the YBCO bridges was taken into account in the numerical simulations of the current–voltage characteristics. Laser scanning microscopy has been applied to visualize the spatial current distribution in the transport channel under injection.

2. Device structure and characterization

Top views and cross-sectional views of the YBCO/PBCO/Au structure are shown schematically in fig. 1 with indication of the current and voltage terminals. A planar geometry of the structure was chosen to provide uniform injected-quasiparticle flow into the YBCO bridge. YBCO and PBCO layers have been grown epitaxially on $SrTiO_3$ substrates both by laser ablation and by sputtering. The top Au layer has been deposited by sputtering. The thickness of the YBCO, PBCO and Au layers is ~80 nm, 0–40 nm, and ~30 nm, respectively. PMMA e-beam photoresist was used to cover the edges of the YBCO strip. The multilayers were structured using standard photolithography and low-power argon or oxygen etching procedures. The width of the bridges varies between 8 and 20 μm. The narrowest part of the bridge is 20 to 30 μm long and is completely covered by the injection contact. The critical temperature T_c of the YBCO layers is 86–89 K. The critical current density J_C of the YBCO bridges is 5×10^5–3×10^6 A/cm^2 at 77 K, indicating a good crystallinity of the films studied. No decrease of J_C has been observed during the multistep fabrication procedure, as well as during a half-year period of storage at room temperature.

In previous studies of the injection effect in controlled weak-link structures [2–4], the length of the narrowest part of the bridge was an order of magnitude larger than the length of the gate. In this case the generated "normal" overheated zone in the gate-contact area propagates along the bridge with thermal speed, yielding a voltage drop proportional to the length of the bridge. The switching time of such a system is in the kHz range and below and the operation mode is latching [2,3]. In the present study we do not create an overheated normal state in order to minimize heating effects. We also restricted the length of the bridge to the length of the gate-contact to clarify the intrinsic behavior of YBCO in the area under injection.

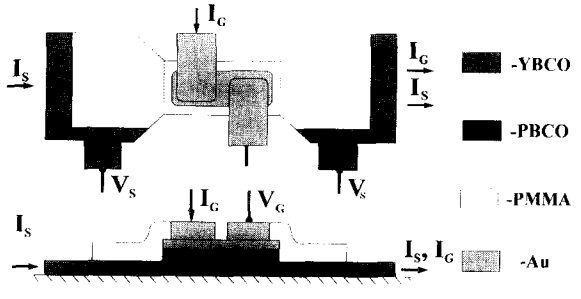

Fig. 1. Schematic view of the YBCO/PBCO/Au structure with the indication of the terminals.

The uniformity of the current distribution of the injected quasiparticles through the junction area should be estimated. The nonuniformity of the current distribution becomes significant if the length of the gate exceeds the transfer length l_t [6]:

$$l_t \sim (R_n A d_{Au}/\rho_{Au})^{1/2}. \quad (1)$$

Here R_nA is the product of the normal-state resistance and the area of the YBCO/Au or YBCO/PBCO/Au contacts, ρ_{Au} is the resistivity of the Au layer and d_{Au} is its thickness. The YBCO/Au contacts have R_nA values of 1–3×10^{-5} Ω cm^2 at $T \leqslant T_c$(YBCO), which increases only 10–20% upon lowering the temperature to 4.2 K. For such contacts l_t is about 200 μm. This is much larger than the length of the contact. Addition of a 20–40 nm PBCO layer, giving rise to YBCO/PBCO/Au structures, changes the $R_n(T)$ behavior. At 80 K we find $R_nA \sim 10^{-4}$–10^{-3} Ω cm^2 and R_nA increases several orders of magnitude upon lowering the temperature to 10 K. For these YBCO/PBCO/Au contacts the value of l_t is even larger. Thus, we may treat the distribution of the injection-current density in the contact area as uniform.

3. Results and discussion

3.1. YBCO/PBCO/Au structures

In fig. 2 we show the critical current I_C of the YBCO bridge as a function of the injection current I_G from the YBCO/PBCO/Au gate contact for different temperatures. For this sample the thickness of the PBCO barrier is 20 nm. Similar $I_C(I_G)$ depen-

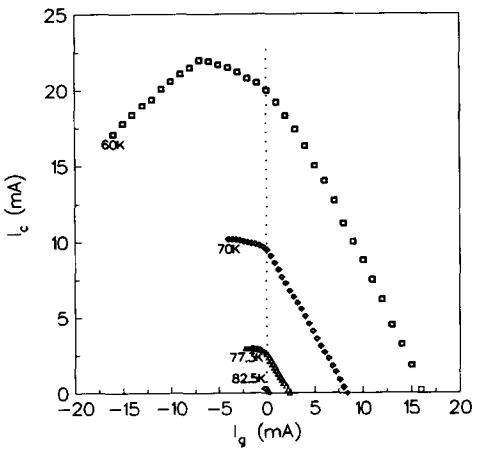

Fig. 2. Dependences of the critical current of the YBCO bridge of YBCO/PBCO/Au structure with a 20 nm thick PBCO barrier on the injection current I_G at several temperatures.

dences are found if the direction of I_S and I_G are both reversed. In the studied temperature range of 60 K to 85 K we find asymmetrical $I_C(I_G)$ dependence – an almost linear suppression of I_C with parallel flow of I_G and I_S and a rather nonlinear dependence for a flow of I_G in the opposite direction of I_S at 60 K. The lower bound of the temperature range for these measurements is determined by the stability of the bridges with respect to large values of the currents I_S and I_G.

The behavior of I_S as a function of the injection current I_G is due to two different effects:
(1) summation of I_S and I_G in the YBCO bridge, and (2) additional nonlinear suppression of I_C with I_G even for an opposite direction of the currents I_S and I_G. The second effect can be attributed to different mechanisms – thermal heating, a nonequilibrium energy spectrum of the injected quasiparticles, injection-enhanced vortex motion, and so on. As we will discuss below, the current-summation effect yields almost a linear suppression of I_S with I_G for the parallel direction of the current flows and no suppression of I_S for the opposite direction of the currents. The current summation effect yields only $K_G \leqslant 1$. We found that in the YBCO/PBCO/Au structures under investigation the contribution of nonlinear effects and the value of K_G depend on the thickness of the PBCO barrier and on the temperature. An increase of the PBCO barrier thickness decreases the current-gain coefficient, if the structures are compared at the same temperature. No current gain $K_G > 1$ was found at large thicknesses of the PBCO barrier. Next, we will analyze the measurements on YBCO/PBCO/Au structures with a 40 nm thick PBCO barrier to describe the current-summation effect. Since the current summation has a similar contribution in all the structures studied, it can be subtracted later from measurements on structures with thinner PBCO barriers in order to extract nonlinear effects under injection.

Figure 3 shows schematically the current-summation effect in the YBCO bridge. The total current density $J = J_S + J_G$ along the YBCO bridge depends on the direction of the injected current with respect to the transport current. If J_S and J_G are parallel, their sum $J_S + J_G$ has a maximum value near the exit of these currents from the junction area, as shown schematically in fig. 3(b). If J_s and J_G are in opposite directions, the maximal density of the total current is on the opposite side of the junction (fig. 3(c)). Thus, even with a uniform current flow of I_G through the contact area, the nonuniformity of the current flow through the YBCO bridge gives different $I_C(I_G)$ dependences for the cases of parallel and opposite direction of the currents I_S and I_G.

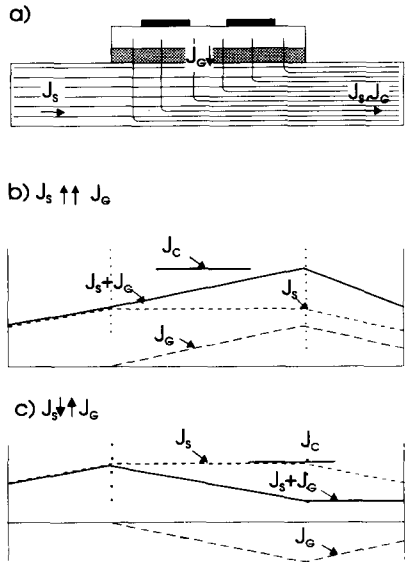

Fig. 3. Schematic model of the current distribution along the YBCO bridge due to the summation of the supercurrent I_S and injection current I_G.

The critical current I_C of the YBCO bridges has been determined with a voltage criterium of 1–2 μV over the bridge length. The analysis of the current–voltage (I–V) characteristics of the bridges under injection yields more detailed information on their behavior. Many competing models have been proposed for the description of the vortex dynamics in HTS's and their I–V characteristics [1,7–11], using e.g. the Anderson–Kim flux-creep model for single vortices or collective effects in the vortex lattice. Figure 4 shows a typical set of I–V characteristics of the YBCO bridge. In a log I–log V plot all curves have a negative curvature. The experimental data in fig. 4 can be fitted rather well to the formula

$$E/J \sim \rho_0 \exp(-(J_0/J)^{\mu}) , \qquad (2)$$

which was predicted both by the collective-creep [10] and vortex-glass [11] model. The parameters μ, ρ_0 and J_0 can be found by fitting of the experimental data to eq. (2). For the data in fig. 4 μ increases from about 1 at 80 K to 1.6 at 65 K. Such values are larger than predicted by both models. Our measurements have been done without applying a magnetic field, which can be a reason for the larger values of the μ coefficients, than that predicted by the models [10,11]. With applying an external magnetic field up to 2 T the I–V characteristics have the same negative curvature in the log I–log V plot and can also be described by eq. (2), but with lower values for μ. For the present analysis we apply eq. (2) only for the description of the change in the I–V characteristics under injection due to the summation of currents in the YBCO bridge. A more detailed comparison of the experimental data with different flux-creep models is not a topic of this article. Together with the behavior of injection-controlled structures in an applied magnetic field it will be discussed elsewhere.

Assuming a uniform injection current over the junction area:

$$J(x) = J_S + J_C(x/L) , \qquad (3)$$

the total voltage drop over the junction length in the presence of the injection current can be written as

$$V \sim \int E(x)\,\mathrm{d}x = \rho_0 \int J(x) \exp(-(J_0/J(x))^{\mu})\,\mathrm{d}x , \qquad (4)$$

where $J(x)$ is given by eq. (3). The resulting I–V characteristics under injection have been found by the numerical evaluation of eq. (4). Figure 5 shows the experimental data (shown by markers) and the calculated curves (solid lines) for the YBCO bridge in YBCO/PBCO/Au structures with a 40 nm thick PBCO barrier at a temperature of 65 K. A reason-

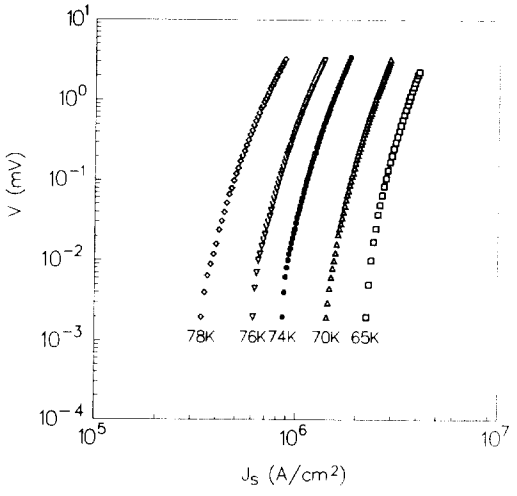

Fig. 4. I–V curves of the YBCO bridge of an YBCO/PBCO/Au structure with a 40 nm thick PBCO barrier at different temperatures.

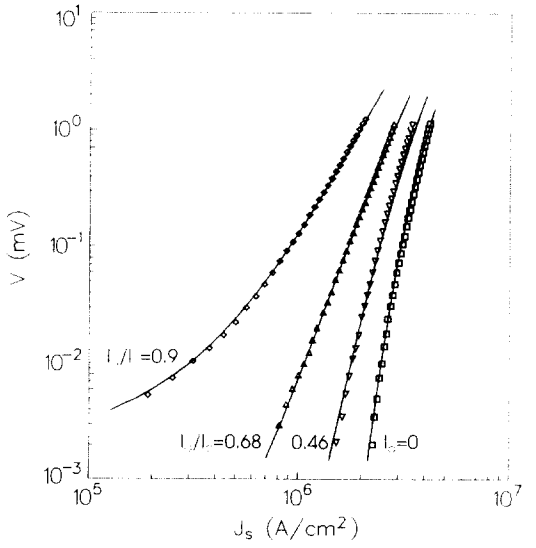

Fig. 5. I–V characteristics of the YBCO bridge of an YBCO/PBCO/Au structure with 40 nm thick PBCO barrier at 65 K with injection current. Experimental data are given by markers, simulated curves are shown by solid lines.

able fit has been found for these structures with the same values of ρ_0, J_0 and μ, as were found for bridges without injection at 65 K. Only for an injection current $I_G = 0.9 I_C$ the value $J_0^* = 0.9 J_0$ has been used. Thus, for thick PBCO barriers the influence of the injection current can be interpreted as a summation effect of the currents I_S and I_G in the YBCO bridge without any significant change in the temperature of the sample and of the substrate T_{bath}.

We have proposed earlier [5] that the I_C suppression is due to a current-summation effect: $\Delta I_C^{sum} \sim I_G$. Simulation of the I–V characteristics by eq. (4) with nonuniform current distribution $J(x)$ also gives a linear dependence of ΔI_C^{sum} on I_G as $\Delta I_C^{sum} \sim 0.85 I_C$. This correction is due to the nonlinear dependence of the voltage on bias current (see eq. (2)).

In this paper we mainly discuss the case in which I_S and I_G are in parallel directions. Taking the current-summation effect in the YBCO bridge into account, the behavior of the structures is rather similar for the parallel and opposite direction of the current I_S, as we discussed earlier [5].

3.2. YBCO/Au structures

The largest current-gain coefficient has been obtained in YBCO/Au structures. Figure 6 shows

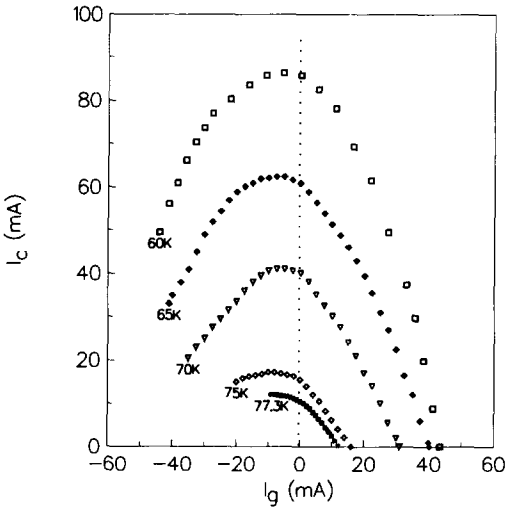

Fig. 6. Dependence of the critical current of the YBCO bridge on the injection current I_G of an YBCO/Au contact at different temperatures.

$I_C(I_G)$ dependences for the YBCO/Au structures at different temperatures. At temperatures close to T_C, we have found a small contribution of nonlinear effects on the $I_C(I_G)$ dependence with $K_G \sim 1$. Lowering the temperature increases K_G, reaching a value of 2 at 60 K. The $I_C(I_G)$ dependences are rather nonlinear in the temperature range of 60–70 K. A current-summation effect suppresses I_C for $I_G > 0$ only linearly. Due to the large current densities, heating of the structure and the substrate could be the reason for the nonlinear $I_C(I_G)$ dependence. Comparing the dissipated power $P_G = I_G V_G$ in the YBCO/Au with that in YBCO/PBCO/Au structures with a thick PBCO barrier, we find that for the YBCO/PBCO/Au structures the absolute value of P_G is larger than that for YBCO/Au structures at similar temperatures. However, in YBCO/PBCO/Au structures at $d_{PBCO} = 40$ nm there is no current gain ($K_G \sim 1$) for temperatures of 60 to 80 K. Thus, heating due to dissipated power is small in such planar structures and cannot explain the large values of K_G in the YBCO/Au structures. For this reason we attribute the current-gain effect to nonequilibrium effects caused by injection.

The current–voltage characteristics of the YBCO/Au structures under injection can also be simulated by eq. (4). Figure 7 shows the experimental data and the simulated curves for the YBCO/Au structures at 65 K. A simulation of the injection effect with values of ρ_0, J_0 and μ estimated for an operating temperature of 65 K for the given YBCO bridge, is shown in fig. 7 as solid line. They are completely different from the experimental data. We attribute this to the nonequilibrium effect under injection. In order to take this into account we assume that the effective temperature T^* of the YBCO bridge increases under injection due to nonequilibrium effects. The effective temperature T^* can be estimated as $I_C(T^*) = I_{C0} - \Delta I_C^{NES}(I_G)$, where the suppression of the supercurrent due to nonequilibrium effects is $\Delta I_C^{NES}(I_G) = \Delta I_C^{tot} - \Delta I_C^{sum} = I_{C0} - I_C(I_G) - 0.85 I_G$ and I_{C0} is the value of the supercurrent I_C at $I_G = 0$. Using the $I_C(T)$ and I–V dependences of the YBCO bridge without injection, we can estimate T^* and the parameters ρ_0^*, J_0^* and μ^* for this effective temperature T^*. This can be done for all injection currents. The calculated I–V characteristics for such parameters and for the $J_C(T^*)$ value are plotted in fig. 7

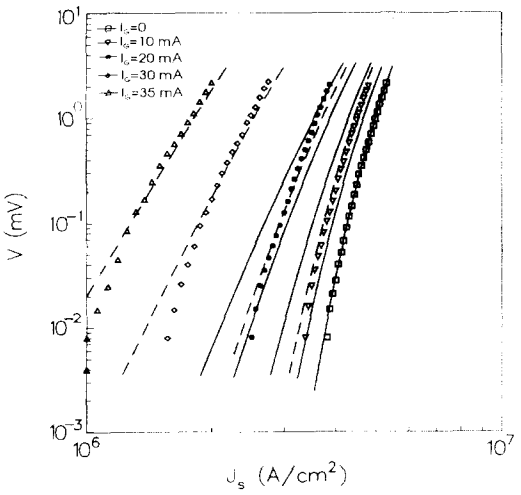

Fig. 7. I–V characteristics of the YBCO bridge of an YBCO/Au structure at 65 K with injection current. Experimental data are given by markers, simulated curves are shown by solid lines for the equilibrium temperature (T=65 K) and by dashed lines for the effective temperature $T^*(I_G)$.

by the dotted lines. The fit is reasonable. It could be improved by a better estimate of the parameters ρ_0^*, J_0^* and μ^* under injection. The main conclusion we draw here is the presence of a significant change in the effective temperature T^* of the YBCO bridge under the quasiparticle injection. For the analyzed structure this means an increase of T^* of ~5–6 K above the temperature of the system of T_{bath}=65 K.

The change of the effective temperature T^* with the injection current I_G for the YBCO/Au structures agrees qualitatively well with the proposed expression from Parker's T^*-heating model [12]:

$$P_G = I_G V_G = c(T^{*4} - T_{bath}^4) , \quad (5)$$

as we discussed in ref. [5]. Here T_{bath} is the equilibrium temperature of the system and c is a coefficient, which depends on the interface-boundary resistance and temperature. Direct application of eq. (5) to the YBCO/PBCO/Au structures should result in larger effects for structures with a thick PBCO barrier. However, only the effective energy of the quasiparticles, which enter the YBCO strip, should be considered in eq. (5). IN YBCO/PBCO/YBCO structures the transport mechanism through the PBCO barrier can be described as variable-range hopping with Lifshitz correlations at low densities of the crystal defects [13,14]. At temperatures of 60 to 80 K the average hopping length of the carriers is several nm in the c-axis direction of PBCO. Thus, at a thickness of the PBCO barrier of 40 nm the resulting energy of the injected quasiparticles can be relatively small, typically 5–10% of the applied bias voltage. The major part of the voltage drop is due to the inelastic motion through the high -resistive PBCO barrier. The situation can be different at very low temperatures (when the hopping length increases quickly) or for a thin PBCO barrier. The YBCO/PBCO/Au planar structures with a thin PBCO barrier are under investigation now.

The nonbolometric increase of the effective temperature T^* suggests a change in the energy spectrum of the quasiparticles in the YBCO bridge under injection. An enhancement of the flux creep under quasiparticle injection in the structures cannot be extracted from the available data and needs further study.

3.3. Laser scanning microscopy

To check the validity of the proposed model it is important to determine the current-density distribution in the measurement area. We have applied laser scanning microscopy to visualize the spatial distribution of the current in the contact area. The principles of this technique have been described elsewhere [15]. Briefly, under laser irradiation the sample is locally heated by approximately 0.1 K. The sample studied is biased just above I_C giving rise to a voltage drop across the bridge of ~10–20 μV. A local change of the current density J in the bridge, caused by local heating by the laser spot, results in a voltage response ΔV. Scanning over the contact area, the spatial distribution of the current density can be recorded. The diameter of the laser beam is ~1 μm and the repetition rate of the laser pulses is ~10 kHz. Figure 8 shows the spatial image of the YBCO/Au structure at 65 K at different ratios of the currents I_G/I_C. The area of the contact is marked by dotted lines for clarity. For structures with a top Au layer some complications in the direct reproduction of the spatial image arise due to the larger reflection of the Au terminals of the injector junction. The image could be restored by taking into account the reflectance coefficient $R(x, y)$ on the junction area.

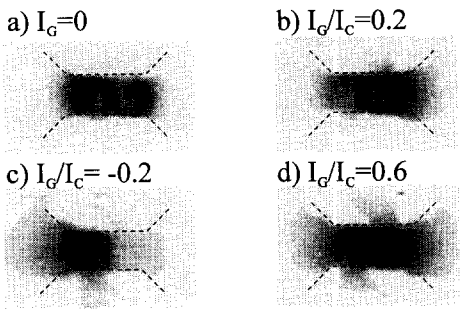

Fig. 8. Visualization of the spatial distribution of the voltage drop over the junction area of the YBCO/Au junction by laser scanning microscopy at different levels and directions of the injected current I_G.

However, even without that we can compare the relative change of the response at different I_G values. Figure 8(a) shows the response of the YBCO/Au structure without injection current ($I_G=0$). For parallel directions of the currents I_S and I_G in the YBCO bridge at 65 K and for small values of I_G/I_C (fig. 8(b), $I_G/I_C=0.2$), the voltage drop is located mainly near the end of the bridge. For the opposite direction of the currents and at low values of the ratio I_G/I_C (fig. 8(c), $I_G/I_C=-0.2$), the main voltage drop is on the opposite side of the bridge. At higher injection levels at 65 K (fig. 8(d), $I_G/I_C=0.8$) the response is much stronger and more uniform over the junction area. For the YBCO/PBCO/Au structures at 65 K the images, shown in figs. 8(b) and (c) have been found for all injection currents.

These observations support the proposed model for the behavior of the structures under quasiparticle injection. At low injection currents for YBCO/Au structures as well as for all currents for YBCO/PBCO/Au structures, the modulation of the supercurrent is mainly due to the current-summation effect in the YBCO bridge channel. At higher levels of the injection for the YBCO/Au structure a more uniform response to the external laser irradiation shows a rather uniform suppression of the supercurrent over the junction area which can be attributed to nonequilibrium effects.

4. Conclusions

The behavior of the injection-controlled YBCO/Au and YBCO/PBCO/Au structures is determined by two effects:

(1) summation of the transport and injected currents in the YBCO bridge, and

(2) nonequilibrium suppression of the supercurrent due to the quasiparticle injection.

No current gain was found at 60–85 K for the YBCO/PBCO/Au structures with a thickness of the PBCO barrier of 40 nm. The PBCO barrier is not effective at such a thickness of the barrier due to the small hopping length of the carriers in the *c*-axis direction of PBCO and extra energy losses in the barrier. Current–voltage characteristics of the YBCO/PBCO/Au structures under injection can be described within the collective-creep or vortex-glass models by the current-summation effect in the YBCO bridge without significant change of the effective temperature of the sample. The YBCO/Au structures show a gain effect $\Delta I_C/\Delta I_G > 1$. The current-gain coefficient increases linearly with lowering temperature, reaching a value of 2 at 60 K. An increase of the effective temperature T^* of these structures agrees qualitatively well with Parker's T^*-heating model. Visualization of the voltage drop over the junction area by laser scanning microscopy is in agreement with the conclusions drawn from electrical measurements with respect to current summation and nonequilibrium effects under quasiparticle injection.

Acknowledgements

The discussions of the results with I.P. Nevirkovets, M.G. Blamire, J.E. Evetts and the assistance of D. Terpstra with the numerical simulations are gratefully acknowledged. These investigations have been supported by the Scientific Foundation of the Netherlands (NWO) and the Foundation for Technology (STW).

References

[1] E. Zeldov, N.M. Amer, G. Koren, A. Gupta, R.J. Gambino and M.W. McElfresh, Phys. Rev. Lett. 62 (1989) 3093.

[2] T.-W. Wong, J.T.C. Yeh and D.N. Langenberg, Phys. Rev. Lett. 37 (1976) 150.

[3] Y. Okabe, P. Anprung, K. Fukuoka and M. Tonouchi, Jpn. J. Appl. Phys. 25 (1986) 1342.

[4] T. Kobayashi, K. Hashimoto, U. Kubasawa and M. Tonouchi, IEEE Trans. Magn. 25 (1989) 927.
[5] Yu.M. Boguslavskij, K. Joosse, F.J.G. Roesthuis, G.J. Gerritsma and H. Rogalla, Proc. of LT-20 Int. Conf., PH-92, Physica B (1993), to be published.
[6] W.M. Loh, S.E. Swirhun, T.A. Schareyer, R.H. Swanson and K.C. Savaswan, IEEE Trans. Electr. Devices ED-34 (1987) 512.
[7] P.W. Anderson and Y.B. Kim, Rev. Mod. Phys. 36 (1964) 39.
[8] Y. Yeshurun and A.P. Malozemoff, Phys. Rev. Lett. 60 (1988) 2202.
[9] R. Griessen, Physica C 172 (1991) 441.
[10] M.V. Feigel'man, V.B. Geshkenbein, A.I. Larkin and M.V Vinokur, Phys. Rev. Lett. 63 (1989) 2303.
[11] M.P.A. Fisher, Phys. Rev. Lett. 62 (1989) 1415.
[12] W.H. Parker, Phys. Rev. B 12 (1975) 3667.
[13] I.Z. Kostadinov and B. Alexandrov, Physica C 201 (1992) 126.
[14] Yu.M. Boguslavskij, M.A.J. Verhoeven, F.J.G. Roesthuis, G.J. Gerritsma and H. Rogalla, Proc. of LT-20 Int. Conf., F9-7, to be published in Physica B (1993).
[15] A.G. Sivakov, A.P. Zuravel', I.M. Dmitrenko, V.G. Volotskaya and O.A. Koretskaya, Sov. J. Supercond. Phys. Chem. Techn. 5 (1992) 1746.